Fundamental Research 5 (2025) 407–418

Contents lists available at ScienceDirect

Fundamental Research

journal homepage: http://www.keaipublishing.com/en/journals/fundamental-research/

Article

End-to-end dataflow engineering framework of honey manufacturing from intermediates to process by TAS1R2@AuNPs/SPCE biosensor coupled with quality transfer principle

Xiaoyan Hu[a,b,c], Jingqi Zeng[a,b,c], Lijuan Ma[b,c], Xiaomeng Wang[b,c], Jing Du[d], Lu Yao[d], Zhisheng Wu[a,b,c,*]

[a] Fujian University of Traditional Chinese Medicine, Fuzhou 350122, China
[b] Engineering Research Center for Pharmaceutics of Chinese Materia Medica and New Drug Development, Ministry of Education, Beijing 100102, China
[c] Beijing University of Chinese Medicine, Beijing 100102, China
[d] China Beijing Tongrentang Group Co., Ltd. Beijing 100062, China

ARTICLE INFO

Article history:
Received 9 June 2022
Received in revised form 18 August 2022
Accepted 19 September 2022
Available online 23 October 2022

Keywords:
End-to-end dataflow
Quality transfer principle
Critical quality attributes
Biosensor
Honey manufacturing

ABSTRACT

This study reported an original end-to-end dataflow engineering framework for the quality transfer principle to overcome the quality challenges in real-world honey manufacturing. Firstly, 650 pivotal data points of physical and chemical quality attributes from 65 batches of honey intermediates were characterized through multiple sensors, which included rheological properties, acidity, moisture, and sugars. Furthermore, a hypersensitized TAS1R2@AuNPs/SPCE biosensor was developed to identify biological quality attributes of honey, the powerful affinities between honey intermediates and the TAS1R2 receptor were discovered ($K_D < 1 \times 10^{-8}$ M), and the abnormal batches of B2, B23 and C23 were diagnosed by TAS1R2@AuNPs/SPCE biosensor and multivariable algorithm. Finally, the end-to-end dataflow containing physical, chemical and biological critical quality attributes was successfully established to interpret the quality transfer principle of honey manufacturing, which revealed that the front-end refining process was relatively unstable and the back-end refining process was a negligible influence on the quality of honey manufacturing. This framework embraces quality management, quality transfer, and biosensor information, which will contribute to discovering the quality transfer principle in industrial innovation for intelligent manufacturing.

1. Introduction

Honey plays a paramount role in the pharmaceutical and food fields [1–4]. The global honey revenue is approximately $769.7 million in 2021 and is expected to reach $1522.9 million in 2028. Honey manufacturing is one of the most popular purification techniques of Chinese patent medicine. In the Pharmacopoeia of the people's Republic of China, about one hundred manufacturing processes of Chinese patent medicine employ honey manufacturing. Since the 21st century, numerous countries have successively released industrial 4.0 and other strategies for new-generation intelligent manufacturing [5–7]. China has emphasized that intelligent manufacturing is the main direction of development [8]. Intelligent manufacturing is integrated between industrialization and information technologies, its essence is the flexible use of digital technologies, design into products, and virtual into reality [9–10].

It is worth mentioning that process quality control is a multiscale challenge and plays an indispensable role in intelligent manufacturing [11]. The pharmaceutical and food industries in particular should pour more attention into their quality issues [12]. Because multitudinous enterprises only focus on measurements but not process control, there are serious problems such as unsubstantial management and inefficiency. To overcome the quality challenges in real-world manufacturing, an end-to-end dataflow engineering framework was innovatively proposed to control the quality of honey manufacturing. The framework adequately answered the following quality questions. (1) How to achieve quality management of honey manufacturing? (2) what affected the quality of honey? (3) How was the quality transferred in honey manufacturing?

For the first quality question, quality management is the significant foundation of honey manufacturing. The U.S. Food and Drug Administration (FDA) has illuminated that the critical quality attributes (CQAs)

* Corresponding author.
E-mail address: wzs@bucm.edu.cn (Z. Wu).

https://doi.org/10.1016/j.fmre.2022.09.029

encompass physical, chemical, biological and microbial characteristics that are typically representative of quality [13]. Both physical and chemical CQAs of honey were strictly prescribed in the Pharmacopoeia of the people's Republic of China, which could be characterized by multifarious sensors, such as visible and near-infrared (Vis-NIR) spectroscopy [14], attenuated total reflection Fourier transform infrared (ATR-FT-IR) [15], mid-infrared (MIR) spectroscopy [16] and so forth. Moreover, biological quality characterization is one of the crucial foundations in honey manufacturing. Recently, biosensors have emerged to identify biological CQAs of other varieties, especially the biomarkers of clinical disease and the affinity between chemical CQAs and targets [13, 17, 18]. Remarkably, the screen-printed carbon electrode (SPCE) as a primary material of biosensors has low consumption, high reproducibility, and convenient operation, which has been extensively employed in the pharmaceutical and food industries [19–21]. Additionally, nanomaterials have excellent electrical conductivity, chemical inertia, and biocompatibility, which can enhance the electrochemical performances of the biosensor, including metal nanoparticles, graphene, etc. [22–24]. The aptamers are modified on the nanomaterial-based SPCE as a recognition element, and biosensing signals are generated through specific interactions of ligands and aptamers [25]. Therefore, the biosensor provides a tremendous opportunity for identifying biological CQAs of honey manufacturing.

Furthermore, characteristic quality information is the heart of the framework. Notably, substantial data are exploding and uneven, which means that digital characteristic information cannot be integrated [26]. For this, multivariate statistical analysis is extensively applied in many fields because it is a high-performance approach that integrates complex data from multiple sources to procure characteristic information [27]. Multivariate statistical process control (MSPC) has unique advantages in-process quality monitoring and controlling in many areas, which can cope with high-dimensional, incomplete, complex, vague and massive datasets by calculating Hotelling T^2 and Q statistics [27–29].

What's more, honey manufacturing is intricate and uninterrupted, which means that its quality is influenced by a series of technologies and factors from raw materials to intermediates and then to products [30]. How to transfer quality from end to end with multi-dimensional CQAs is an intractable nodus. Notably, multivariate path analysis of intelligent manufacturing can represent the causality between multiple independent variables and dependent variables, which is an extension of regression analysis and can handle relatively complex variable relationships [27]. Therefore, the framework can perfectly interpret the end-to-end quality transfer principle in real-world honey manufacturing.

Here, to overcome the quality challenges in honey manufacturing, we developed the engineering framework. Specifically, it consisted of three critical elements. Firstly, the TAS1R2@AuNPs/SPCE biosensor was assembled and combined with several sensors to characterize quality attributes. Secondly, the quality management strategies from the physical, chemical and biological CQAs were established by Scatterplot Matrices and MSPC. Finally, end-to-end quality transfer dataflow was developed, which further elucidated the quality transfer principle in honey manufacturing. Real-world honey manufacturing from intermediates to processes is thus taken as our research object, which will provide credible methodological and theoretical guidance for intelligent manufacturing.

2. Materials and methods

2.1. Instruments and materials

The physical quality attributes of honey intermediates were characterized by a HAAKE Viscotestecr IQ rotary rheometer (ThermoFisher, America) ; the chemical quality attributes of honey intermediates were characterized by PHS-3E digital display benchtop pH meter (Electrical Scientific Instrument, China), 1260 High-performance liquid chromatography (HPLC) with the evaporative light scattering detector (ELSD) (Agilent, America) and 2WAJ Monocular Abbe refractometer (Lichen Bangxi Instrument Technology, China); the biological quality attributes of the honey intermediates were characterized by a CHI660E electrochemical workstation (Chenhua Instrument, China) and SPCE (Glass Carbon Technology, China).

There were 5 batches of raw honey (A1, A2, …, A5), 30 batches of refined honey (B1, B2, B3, …, B30) and 30 batches of he-tuo honey (C1, C2, C3, …, C30) from the intermediates of the Tongren Niuhuang Qingxin pills in the manufacturing process, provided by China Beijing Tongrentang Group Co., Ltd. Fructose (98.0% mass fraction, st109001), glucose (98.0% mass fraction, st052501), sucrose (98.0% mass fraction, st202101), and maltose (98.0% mass fraction, st215001). All reference substances were purchased from Shanghai Shidande Standard Technical Service Co., Ltd. (China); the taste receptor type 1 member 2 (TAS1R2) was provided by CrystalO Biopharma Technology Co., Ltd. (China); Chromatographic methanol and Chromatographic acetonitrile were purchased from Thermo Fisher Scientific Co., Ltd. (America); Phosphate-buffered solution (PBS, pH 7.4), potassium chloride (KCl), potassium ferricyanide ($K_3[Fe(CN)_6]$) and chloroauric acid ($HAuCl_4$) were all provided by Beijing Enokai Technology Co., Ltd. (China); 3-Mercaptopropionic acid (3-MPA), N–Hydroxysuccinimide (NHS) and 1-(3-Dimethylaminopropyl)−3-ethylcarbodiimide hydrochloride (EDC) were purchased from Beijing Zhongnong Boxin Technology Co., Ltd. (China).

2.2. Methods

2.2.1. Physical quality attributes characterization for real-world honey intermediates

Real-world honey is a Newtonian fluid, so rheological properties belong to its physical quality attributes [31]. In the polymerization process, its rheological properties directly affect the adhesion of honey, which include dynamic viscosity (DV), complex viscosity (CV), viscous modulus (VM), and elastic modulus (EM). Here, the rheological properties of honey intermediates were determined by the optimization method in our group's previous experiments.

The DV of honey intermediates was determined in the rotation mode at a shear rate of 50 S^{-1} and 30 ˚C; the CV, VM and EM were determined at 50% shear strain, shear frequency of 5 Hz, and 30 ˚C. The pivotal data points of the physical quality attributes are recorded in Table S1 of the supplementary materials.

2.2.2. Chemical quality attributes characterization for real-world honey intermediates

Acidity is a paramount indicator of honey fermentation, the researchers used pH value as a representative of the activity of hydrogen ions to reflect the acidity of honey, it usually varies with the change of moisture content, sugar concentration, and storage conditions [32, 33]. Moisture is the central chemical quality attribute for determining the endpoint of the honey refining process. Fructose, glucose, sucrose and maltose are the fundamental chemical CQAs of honey intermediates. Moisture content is closely related to sugar content [34]. Their contents and acidity (pH values) were measured by the optimization method in our group's previous experiments.

According to the provision of moisture determination in the Pharmacopoeia of the people's Republic of China, an Abbe refractometer was used to determine the refractive index at 40 ˚C ± 0.1 ˚C, and then the moisture content of the above honey intermediates was calculated by a universal formula Eq. S1. Next, the pH value of honey intermediates was determined through the operating regulations of the pH meter.

The contents of fructose, glucose, sucrose and maltose were determined by HPLC, which included the optimization of chromatographic conditions, the preparation of sample solutions, the preparation of the mixed standard solution, and the detection of sugar content. The specific

steps were recorded in the Supplementary Materials and the pivotal data points on chemical quality attributes were recorded in Table S2.

2.2.3. The development of the TAS1R2@AuNPs/SPCE biosensor

TAS1R2 is a protein in humans, which is encoded by the TAS1R2 gene, and it's also a taste receptor that can recognize diverse natural and synthetic sweeteners such as sucrose, fructose, saccharin, and so on [35–37]. Therefore, the functionalized biosensor of the TAS1R2 protein provided cutting-edge technical support for sugar-rich honey.

Here, the TAS1R2 receptor was coupled to the SPCE and selected as the molecular recognition element; the CHI660E electrochemical workstation was the signal transducer. Initially, the SPCE was exposed to the saturated Na_2CO_3 solution and pretreated for 5 min at 1.2 V by chronoamperometry to remove the organic adhesive. The specific establishment steps of the TAS1R2@AuNPs/SPCE biosensor were as follows.

Firstly, 60 μL of 2.5 mmol·L^{-1} $HAuCl_4$ solutions were dropped onto the working electrode surface of the SPCE. The Au^{3+} was reduced to Au by cyclic voltammetry (CV) scanning dozens of times at a range from −1.5 V to 0 V. Secondly, the surface of AuNPs/SPCE was covered by 10 mmol·L^{-1} 3-MPA aqueous solution and socked at room temperature for 17 h to 24 h, the Au-S bonds were generated on the surface of AuNPs/SPCE. Then, the residual 3-MPA aqueous solution was cleaned with PBS solution, and a 30 μL equal volume mixture of 20 mmol·L^{-1} EDC and 50 mmol·L^{-1} NHS was dropped onto the working electrode surface and reacted for 15 min to activate carboxyl groups. Finally, the TAS1R2 receptor was modified at 4 °C for 2 h to 5 h on the working electrode surface to generate a TAS1R2@AuNPs/SPCE biosensing chip. An electrochemical workstation and a Nicolet iS10 Fourier infrared spectrometer (Thermo-Fisher, America) were used to verify whether the TAS1R2 receptor was successfully modified.

The TAS1R2@AuNPs/SPCE chip was exposed to PBS solution that contained 10 mmol·L^{-1} $[Fe(CN)_6]^{3-}$ and 0.1 mol·L^{-1} KCl for detection by differential pulse voltammetry (DPV). The biosensing signals were used to determine the electrochemical performances of the TAS1R2@AuNPs/SPCE biosensor, which included response time, sensitivity, reproducibility, and stability.

2.2.4. Measurement of representative sugars in honey by TAS1R2@AuNPs/SPCE biosensor

Eight concentrations of glucose and sucrose gradients ranging from 1 nmol·L^{-1} to 10 mmol·L^{-1} were determined by the TAS1R2@AuNPs/SPCE biosensor. 0.2 mol·L^{-1} PBS solution containing 10 mmol·L^{-1} $[Fe(CN)_6]^{3-}$ and 0.1 mol·L^{-1} KCl was used as a blank reagent. The above analytes from low concentration to high concentration were detected by DPV, and the individual test was repeated 5 times. Finally, the affinities between glucose and sucrose with the TAS1R2 receptor were expressed by the dissociation constant (K_D) [38]. The calculation formulae of K_D value could be seen in supplementary material, which included Eq. S2, Eq. S3, and Eq. S4.

2.2.5. Measurement of honey intermediates by TAS1R2@AuNPs/SPCE biosensor

The refined honey and he-tuo honey were configured as the solution with gradients ranging from 2 pg·mL^{-1} to 200 mg·mL^{-1}, which converted to glucose concentration from 0.1 nmol·L^{-1} to 1 mmol·L^{-1}. These solutions were detected from low concentration to high concentration by the TAS1R2@AuNPs/SPCE biosensor. Then, the K_D values of the interaction between the TAS1R2 receptor and honey intermediates were calculated by Eq. (S2), Eq. (S3), and Eq. (S4). Meanwhile, the affinities of the TAS1R2 receptor and sugars were further verified by the LibDock in Discovery Studio (Beijing Chuangteng Technology Co., Ltd., China). In this study, the precise structure of the TAS1R2 receptor was downloaded from the Uniport open-source website, and the similarity and homology of the TAS1R2 receptor in the human body and TAS1R2 structure were as high as 95% in the database.

2.2.6. Characterization of honey intermediates by TAS1R2@AuNPs/SPCE biosensor combined with the multivariable algorithm

Refined honey and he-tuo honey samples were configured as identical concentrations, the working fluid served as the blank control group, and the injection volume was 60 μL. What's more, the parameters of DPV remained unchanged, all samples were scanned 5 times to procure the average signal, and the specific parameters of DPV were recorded in the Supplementary Materials. Then, the biosensing current values were preprocessed and their eigenvalues were extracted by principal component analysis (PCA). Furthermore, the Hotelling T^2 and Square Prediction Error (SPE) models of the MSPC were utilized to achieve an abnormal diagnosis of batch-to-batch honey intermediates. Here, the Hotelling T^2 and SPE statistics were calculated by the Unscrambler X 10.4 (CAMO, USA).

2.2.7. Quality transfer modalities in the honey manufacturing

The pivotal data points of physical, chemical and biological quality attributes in honey intermediates were procured from Sections 2.2.1, 2.2.2, and 2.2.6. Thereinto, the physical quality attributes included four types of rheological properties; the chemical quality attributes included pH value, moisture content and four types of sugar content; the biological quality attributes included affinities between analytes and TAS1R2 receptor, which were indicated by biosensing current values. Finally, the quality transfer modalities from raw honey to refined honey and raw honey to he-tuo honey were interpreted by kernel density estimation (KDE) and box plot.

2.2.8. End-to-end dataflow for quality transfer in honey manufacturing

The pivotal data points of physical, chemical and biological CQAs in honey intermediates were standardized from zero to one to eliminate the dimensional difference between different CQAs. The eigenvalues were extracted by PCA to represent the quality information of honey. The weighted average of the principal component load coefficient was calculated by Eq. (S5) to characterize the relationship between the CQAs and intermediates, their relationship was evaluated by the contribution rate. Ultimately, the original end-to-end dataflow for quality transfer was developed in honey manufacturing.

3. Results and discussion

3.1. Digital characterization based on the physical and chemical quality attributes of honey intermediates

Digital characterization strategies of physical and chemical quality attributes from 5 batches of raw honey, 30 batches of refined honey and 30 batches of he-tuo honey in real-world manufacturing were successfully established through the Scatterplot Matrix with a 95% confidence interval, and the physical and chemical CQAs of honey intermediates were further accurately discovered.

3.1.1. Digital characterization of honey intermediates by physical quality attributes

The physical quality attributes were sequentially characterized, which included DV, CV, VM and EM from the above three types of honey intermediate in real-world manufacturing (Fig. 1a1-a3). From this evidence, the rheological properties of the above three types of honey intermediates varied dramatically in individuals, and their RSD values were up to 25.00%.

Furthermore, according to the histogram of the Matrix scatter plot, the DV and EM of honey intermediates were normal distribution, and different batches were clustered into one category. The DV, PV, VM and EM in raw honey were all within 95% confidence intervals, which indicated that there was no remarkable fluctuation (Fig. 1a1). Noteworthily, it showed that the DV and EM of the B8 and C8 batch exceeded the 95% confidence intervals of their measurements. The honey intermediates

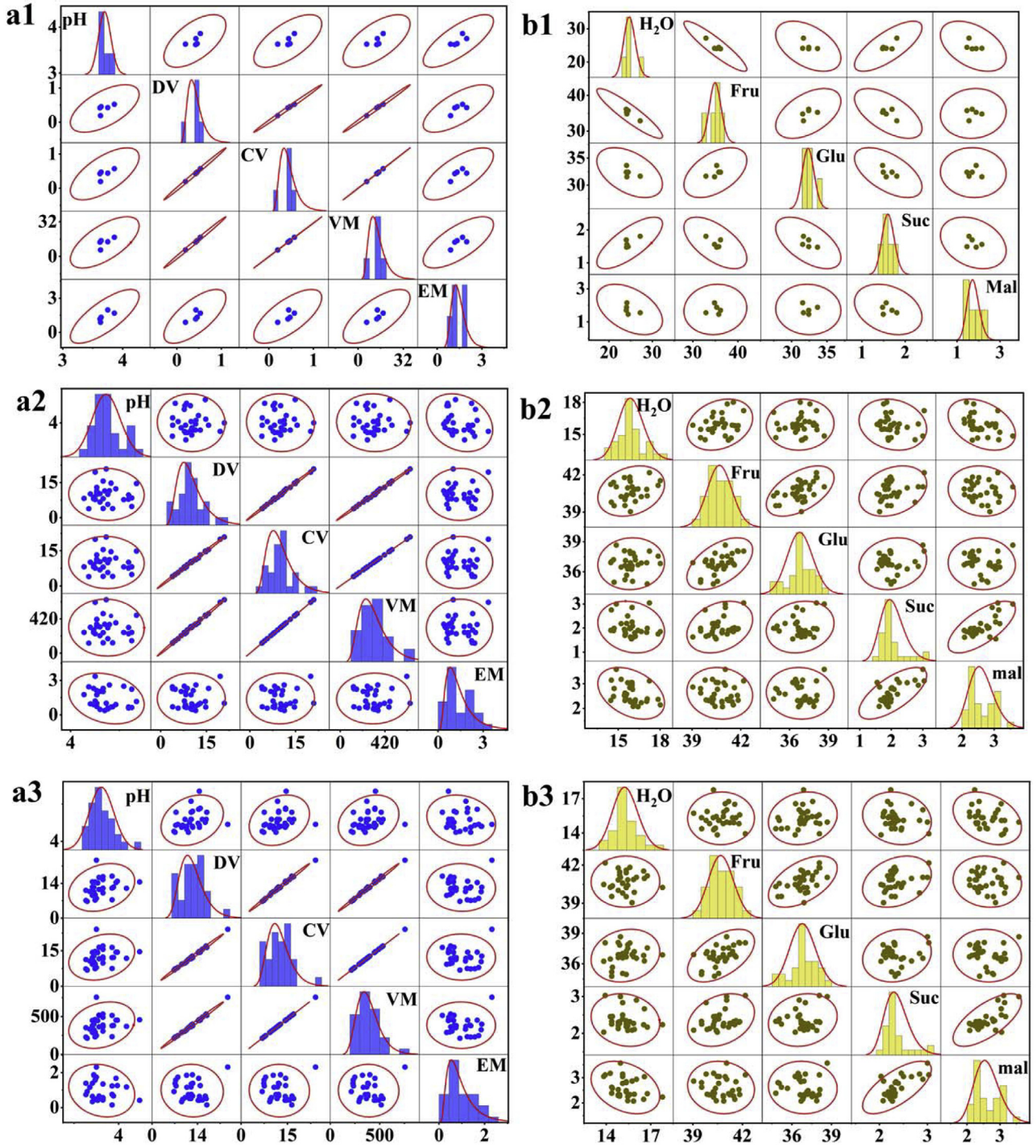

Fig. 1. Phenogram of honey intermediates by the physical and chemical quality attributes (where the abscissa has the same meaning as the ordinate). (a1) Distribution of pH, DV, CV, VM, EM in raw honey. (a2) Distribution of pH, DV, CV, VM, EM in refined honey. (a3) Distribution of pH, DV, CV, VM, EM in he-tuo honey. (b1) Distribution of moisture, fructose, glucose, sucrose and maltose in raw honey. (b2) Distribution of moisture, fructose, glucose, sucrose and maltose in refined honey. (b3) Distribution of moisture, fructose, glucose, sucrose and maltose in he-tuo honey.

corresponding to the above batches were inconsistent with that of others (Fig. 1a2, a3). Therefore, we discovered the physical CQAs affecting the honey intermediates, which included dynamic viscosity and elastic modulus.

3.1.2. Digital characterization of honey intermediates by chemical quality attributes

The chemical quality attributes included pH value, moisture, fructose, glucose, sucrose and maltose from three types of honey intermediates, which were characterized by the Scatterplot Matrix, respectively (Fig. 1b1-b3). From this evidence, the pH values of raw honey, refined honey and he-tuo honey were distributed in the range of 3.62% to 3.86%, 3.78% to 4.11%, and 3.83% to 4.24%, respectively. Specifically, the pH values presented an upward tendency throughout the honey refining process, while the difference between batches was inconspicuous, and their RSD values were all less than 3.00%. It was obvious that the moisture content decreased continuously, while the sugar content increased gradually in honey manufacturing which was more than 70%.

The moisture content of refined honey ranged from 14.46% to 18.01% and the RSD value was 5.54%, and that of he-tuo honey ranged from 14.26% to 17.43%. Therefore, we first observed that the upper-value limit of this range in refined honey had exceeded the real-world standard, and the high moisture content of refined honey affected the stability of production. Meanwhile, we discovered that the moisture content of he-tuo honey corresponded with the production specifications of honeyed pills.

In addition, the distribution histogram indicated that the moisture content was a normal distribution, and different batches were clustered into one category. Meanwhile, the contents of moisture, fructose, glucose, sucrose and maltose in raw honey and refined honey were within the 95% confidence interval, which proved that there was no statistical significance in the chemical quality attributes of raw honey and refined honey (Fig. 1b1, b2). Conversely, one of the 30 batches in he-tuo honey exceeded the 95% confidence interval, which manifested that the pH value of the C30 batch and the moisture content of the C12 batch were remarkable distinction from the others (Fig. 1b3). Throughout the honey refining process, the negative correlation between moisture content and sugar content was discovered to further evidence that pH value, moisture, fructose, glucose, sucrose and maltose were the chemical CQAs of honey intermediates.

In conclusion, we consumed substantial resources to accumulate 650 pivotal data points for physical quality attributes and chemical quality attributes in real-world honey manufacturing. Furthermore, the 95% confidence intervals were constructed by Scatterplot Matrix to successfully achieve the digital characterization of the honey intermediate. Ultimately, we found that the DV, EM, pH value, moisture, fructose, glucose, sucrose and maltose were the CQAs that affected honey manufacturing.

3.2. Development of an innovative TAS1R2@AuNPs/SPCE biosensor

Since the above results showed that the sugar content of honey accounted for approximately 70%, the biological CQAs were characterized by the affinities between the TAS1R2 receptor and honey intermediates. Therefore, we assembled an innovative TAS1R2@AuNPs/SPCE biosensor to characterize the biological CQAs of honey. The development of TAS1R2@AuNPs/SPCE biosensor generally included parameters optimization and performance investigation.

3.2.1. Parameters optimization of the TAS1R2@AuNPs/SPCE biosensor

The establishment procedures of TAS1R2@AuNPs/SPCE biosensor primarily included the gold deposition process, self-assembly process, cross-linking process, and receptor modification process (Fig. 2a). Thereinto, the nano-gold deposition process and the receptor modification process were the most critical procedures. Here, the gold deposition time and receptor modification were optimized progressively.

The electrodeposition times persistently increased and the current peak values displayed a tendency to increase initially and decrease afterward, the current peak value was strongest at the 90th cycle, hence the nano-gold electrodeposition times were specified at 90 in subsequent experiments (Fig. 2b). After the modification of gold nanoparticles, we discovered that the current peak value of AuNPs/SPCE was significantly stronger than that of SPCE, and their peak shapes of the electrical signals were more symmetrical. Additionally, the current peak value of the biosensor chip decreased after the TAS1R2 receptor was successfully modified.

Moreover, compared with SPCE, AuNPs/SPCE could be covalently conjugated with the TAS1R2 receptor by crosslinking 3-MPA. As shown in Fig. 2c, the current peak value of TAS1R2@SPCE was only reduced by 9.07×10^{-6} A when the receptor was covered directly on the surface of SPCE. However, the current peak value of TAS1R2@AuNPs/SPCE was reduced by 4.97×10^{-5} A when the receptor was chemically modified on the surface of AuNPs/SPCE. To further demonstrate the success of TAS1R2 receptor modification, we used Fourier infrared spectrometer to characterize different modified biosensor chips, as shown in Fig. s1, the TAS1R2@AuNPs/SPCE detected strong absorbability at about 1735 cm^{-1} when the presence of an ester group (-COOR).

The above results demonstrated that the modification of gold nanoparticles not only enhanced the conductivity but also improved the TAS1R2 receptor carry capacity of the biosensor chip, and finally the TAS1R2@AuNPs/SPCE biosensor was successfully developed by self-assembly technology.

3.2.2. Electrochemical performances of the TAS1R2@AuNPs/SPCE biosensor

The electrochemical performances of the TAS1R2@AuNPs/SPCE biosensor were investigated by the electrical signal, which included response time, sensitivity, repeatability, and stability. Firstly, the current values of analytes gradually stabilized when the scanning time exceeded 50 s, and that of refined honey and he-tuo honey remained unchanged after 400 s (Fig. 2d). Therefore, the response time was specified at 50 s, and the detection time of the interaction between analytes and TAS1R2 was 400 s. Secondly, 1 $mmol{\cdot}L^{-1}$ glucose solution was determined under different sensitivities (Fig. 2e), which manifested that the electrical signals were powerful and the peak shapes were symmetrical when the TAS1R2@AuNPs/SPCE biosensor performed within the range of 10×10^{-2} A/V to 10×10^{-4} A/V. Furthermore, the aforementioned glucose solution was detected by the TAS1R2@AuNPs/SPCE biosensor and repeated 6 times, the RSD value was 2.3%, so the TAS1R2@AuNPs/SPCE biosensor had satisfactory repeatability (Fig. 2f). The stability of the biosensor was investigated by electrical signals for 5 days (Fig. 2g), the RSD value of 5-day current peak value (I_p, A) was 2.9%, and the TAS1R2@AuNPs/SPCE biosensor fluctuated significantly after 2 days. Therefore, the TAS1R2@AuNPs/SPCE biosensor possessed excellent stability and was recommended to be used within 2 days to avoid experimental errors.

3.3. Characterization of the TAS1R2@AuNPs/SPCE biosensor in honey intermediates

3.3.1. Interaction of representative sugars with TAS1R2@AuNPs/SPCE biosensor

Glucose and sucrose as representative sugars of honey were selected to explore the interactions between sugars and the TAS1R2 receptor, and their interactions were digitally characterized through TAS1R2@AuNPs/SPCE biosensor (Fig. 3a1), the current peak values increased at first and then decreased with the increase of glucose concentration. Ultimately, the common logarithm of glucose concentration and the relative variation value of current peak ($(Ip_n\text{-}Ip_0)/Ip_0$) presented a satisfactory linear relationship in the range from 1 $nmol{\cdot}L^{-1}$ to 10 $\mu mol{\cdot}L^{-1}$ (Fig. 3a2), and the linear regression equation was y=–0.0364x–0.4963 (R^2=0.9415); In the above-mentioned range, glucose concentration ([Ag]) and the ratio of concentration to current variation value ([Ag]/(Ip_n-Ip_0)) also formed an excellent linear relationship (Fig. 3a3) with a linear regression equation of y = 44620x+0.0035 (R^2=0.9992).

Furthermore, the interaction between sucrose and the TAS1R2 receptor was digitally represented through the TAS1R2@AuNPs/SPCE biosensor (Fig. 3b1). The current peak value gradually reduced to a steady state with the increase in sucrose concentration. In addition, the relationship between the base-10 logarithm of sucrose concentration and the relative variation value of the current peak presented a great linear relationship in the range from 1 $nmol{\cdot}L^{-1}$ to 10 $\mu mol{\cdot}L^{-1}$ (Fig. 3b2), and the linear regression equation was y=–0.0408x–0.669 (R^2=0.9570); sucrose concentration and the ratio of concentration to current variation value also formed a perfect linear relationship in the above-mentioned range (Fig. 3b3), and the linear regression equation was y = 19446x+0.0004 (R^2=0.9999).

Ultimately, the K_D values of the interactions of glucose and sucrose with the TAS1R2 receptor were calculated as 7.8440×10^{-8} M and

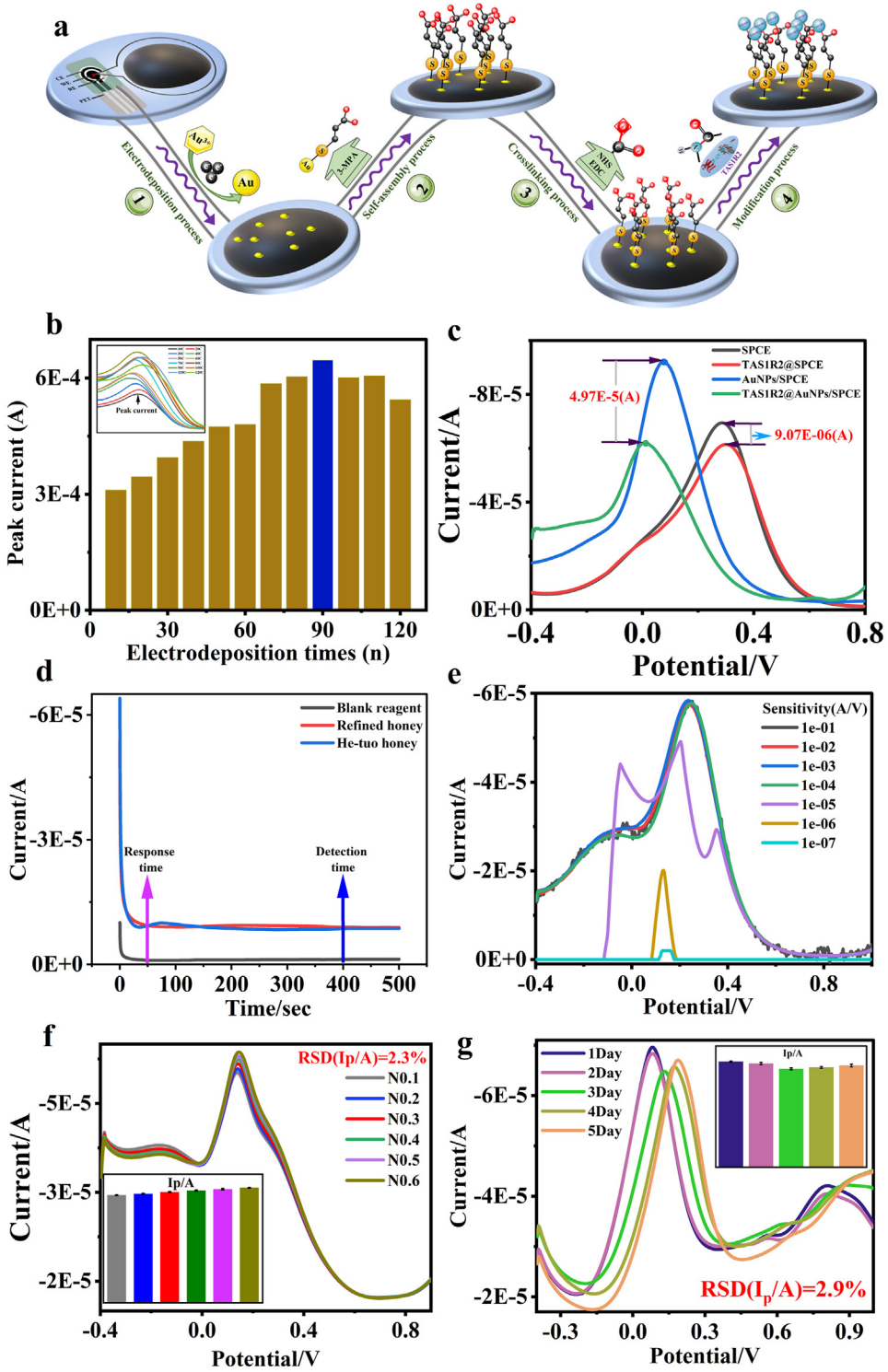

Fig. 2. Diagram of biosensor construction and optimization. (a) Schematic diagram of TAS1R2@AuNPs/SPCE biosensor chip. (b) Optimization graph of gold nanoparticles deposition times. (c) The current response graph of SPCE, gold nanomaterial-based SPCE, TAS1R2 receptor-modified SPCE, gold nanomaterial and TAS1R2 receptor-modified SPCE. (d) Investigation diagram of response time. (e) Investigation diagram of sensitivity. (f) Investigation diagram of reproducibility. (g) Investigation diagram of stability.

2.0570×10^{-8} M, respectively. Therefore, we proved that the representative sugars of honey and the TAS1R2 receptor had powerful affinities.

3.3.2. Interaction of honey intermediates with TAS1R2@AuNPs/SPCE biosensor

The interaction between refined honey and the TAS1R2 receptor was represented in Fig. 3c1. In the range from 1 μmol·L^{-1} to 10 mmol·L^{-1}, the electrochemical signals clustered into a bunch, and the current peak value showed a reversal point at a concentration of 10 mmol·L^{-1} (Fig. 3c2). Remarkably, the common logarithm of concentration and the relative variation values of the current peak presented a satisfactory linear relationship in the range from 0.1 nmol·L^{-1} to 1 μmol·L^{-1}, the linear regression equation was y=–0.0571x–0.704 (R^2=0.9603); In the identical concentration range, the concentration and the ratio of concentra-

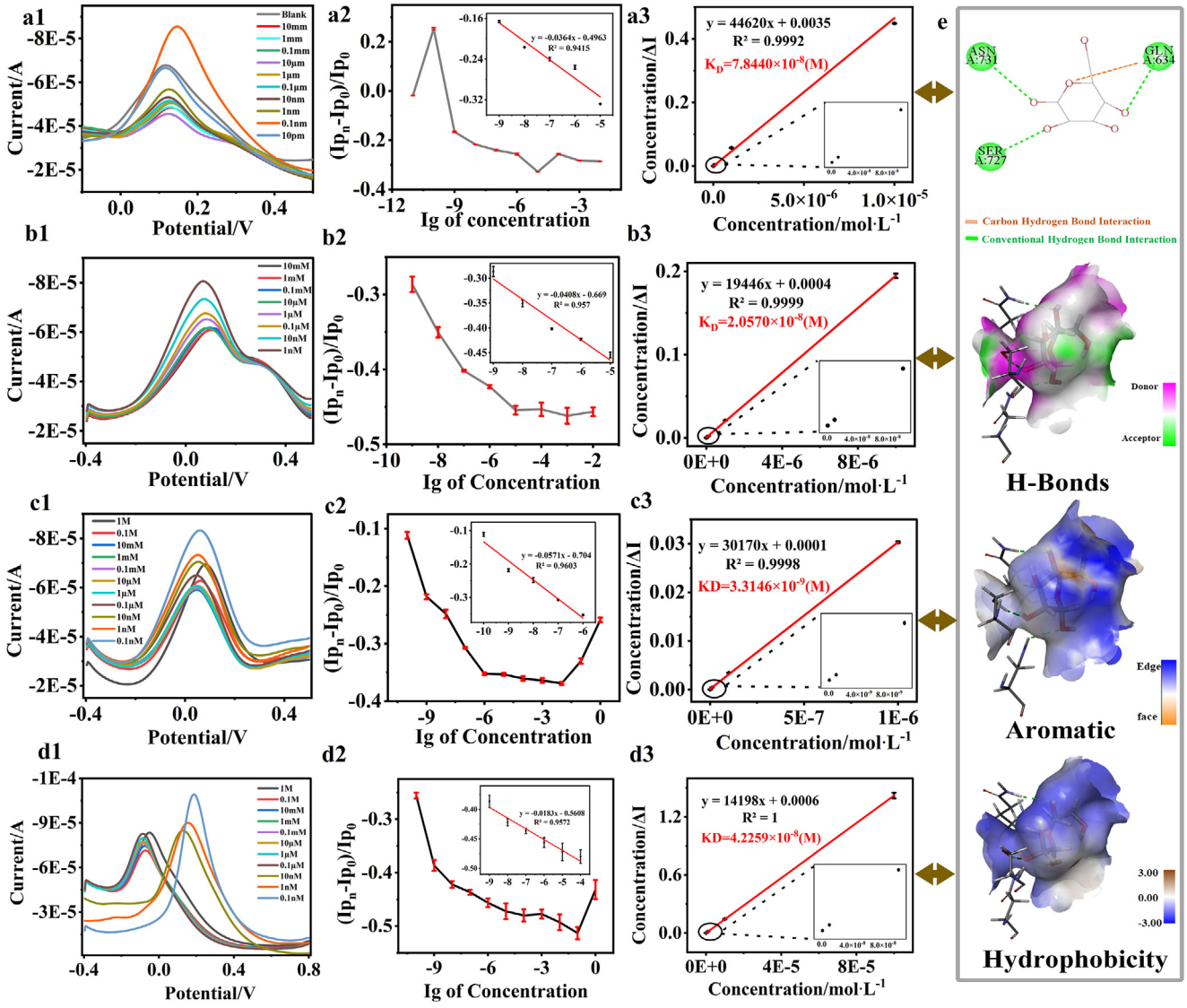

Fig. 3. Diagram of interaction between analytes and TAS1R2 receptor. (a1, b1, c1, d1) *I-V* curve diagrams of the interaction of the TAS1R2 receptor with glucose, sucrose, refined honey and he-tuo honey, respectively. (a2, b2, c2, d2) The linear relationship graphs between the common logarithm of concentration and the relative variation values of the current peak of glucose, sucrose, refined honey and he-tuo honey, respectively. (a3, b3, c3, d3) The linear relationship graphs between the concentration and the ratio of concentration to current variation values of glucose, sucrose, refined honey and he-tuo honey, respectively. (e) 2D and 3D diagrams of macromolecular docking between glucose and TAS1R2 receptor.

tion to current variation value also formed an accurate linear relationship (Fig. 3c3), the linear regression equation was $y = 30170x+0.0001$ ($R^2 = 0.9998$).

Then, he-tuo honey and the TAS1R2 receptor produced a powerful interaction through TAS1R2@AuNPs/SPCE biosensor (Fig. 3d1), the peak current decreased and the peak voltage shifted with the increase of concentration, and it showed a reversal point at a concentration of 0.1 mol·L^{-1}. Notably, the common logarithm of concentration and the relative variation value of the current peak presented a super-duper linear relationship in the range from 1 nmol·L^{-1} to 1 mmol·L^{-1} (Fig. 3d2), and the linear regression equation was $y = -0.0183x-0.5608$ ($R^2 = 0.9572$); the concentration of he-tuo honey and the ratio of concentration to current variation value also formed an exact linear relationship in the same concentration range (Fig. 3d3), and the linear regression equation was $y = 14198x+0.0006$ ($R^2 = 1.0000$).

Eventually, the K_D value of the interaction between refined honey and the TAS1R2 receptor was calculated as 3.3146×10^{-9} M; the K_D value of the interaction between he-tuo honey and the TAS1R2 receptor was 4.2259×10^{-8} M. Therefore, the binding capacities of TAS1R2 receptor and honey intermediates were extremely powerful.

Furthermore, the interactions between the sugars of honey and the TAS1R2 receptor were demonstrated by molecular docking. Here, the glucose-receptor interaction analysis was used as an illustration (Fig. 3e). This evidence further verified that sugars could bind to multiple active pockets of the TAS1R2 receptor, and the binding scores were higher than 72.5355; the combining capacity between sucrose and the TAS1R2 receptor was the most powerful, followed by maltose, glucose, and fructose. This was consistent with the dissociation constants obtained through the biosensor experiment. Additionally, the mechanism of interactions between the TAS1R2 receptor and sugars was explained by their hydrophilicity, hydrophobicity, and hydrogen bond; the primary interaction force was generated by the conventional and carbon-hydrogen bonds, aromatic bonds at the edge, and hydrophilic bonds.

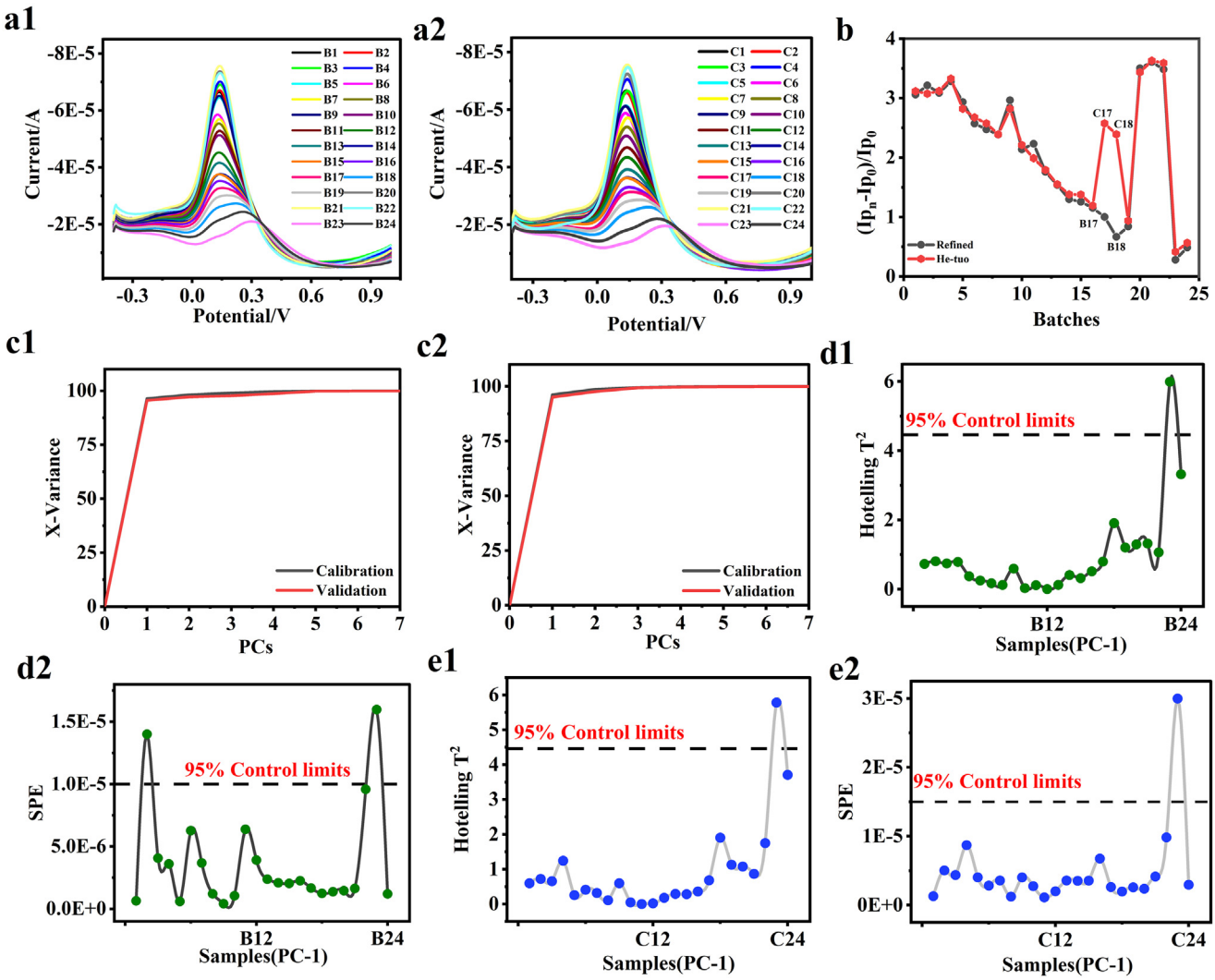

Fig. 4. Diagnostic diagram of honey intermediates through the biosensor and MSPC. (a1, a2) *I-V* curve diagram of refined honey and he-tuo honey by the TAS1R2@AuNPs/SPCE biosensor. (b) Comparison chart of relative variation values of the current peak between refined honey and he-tuo honey. (c1, c2) Variance map of principal constituent factors between refined honey and he-tuo honey. (d1, d2) Hotelling T^2 control diagram and SPE control diagram of refined honey. (e1, e2) Hotelling T^2 control diagram and SPE control diagram of he-tuo honey.

3.4. Diagnosis of honey intermediates by TAS1R2@AuNPs/SPCE biosensor and multivariate algorithm

Multi-batch measurements of honey intermediates were performed by TAS1R2@AuNPs/SPCE biosensor. Their concentration was configured as 0.1 μmol·L^{-1} so that it generated a strong response signal without reaching saturation. The biological signals through the interaction between honey and the TAS1R2 receptor were converted into electrochemical signals. Furthermore, the current value in the range from −0.4 V to 1 V was statistically analyzed by the MSPC algorithm, and the abnormal batches of refined honey and he-tuo honey were specifically diagnosed.

3.4.1. Measurements for honey intermediates by TAS1R2@AuNPs/SPCE biosensor

Refined honey and he-tuo honey were determined by the TAS1R2@AuNPs/SPCE biosensor (Fig. 4a1, a2), and the current peak values varied significantly and their RSD values were greater than 30%. The peak potentials shifted slightly and were then kept unchanged during biosensor detection.

After subtracting the background, the relative variation values of the current peak presented normal distribution. Then the two groups were statistically analyzed and the p-value exceeded 0.05 under the condition of variance homogeneity, which proved that there was no significant distinction. Nevertheless, there was a tremendous fluctuation between the refined honey of B17 and B18 and the he-tuo honey of C17 and C18 (Fig. 4b). It was challenging to accurately predicate the discrete samples of multiple batches by a single variable, accordingly, a multivariable algorithm was introduced to deal with the biosensor multi-information.

3.4.2. Diagnosis of honey intermediates by TAS1R2@AuNPs/SPCE biosensor combined with the multivariate algorithm

Subsequently, the biosensing current values from −0.4 V to 1 V were preprocessed by normalization, and then the eigenvalues were extracted exactly and efficiently by PCA. Surprisingly, the PC1contribution rates of refined honey and he-tuo honey were up to 96% (Fig. 4c1, c2), so the PC1 perfectly replaced their biosensing information. Therefore, the PC1 eigenvalue was used to establish the quality diagnostic model by the MSPC algorithm.

In these models, the refined honey of B2 and B23 exceeded the 95% control limit of the SPE, and B23 also exceeded the 95% control limit of the Hotelling T^2 (Fig. 4d1, d2). Furthermore, the C23 of he-tuo honey was beyond the 95% control limit of Hotelling T^2 and SPE (Fig. 4e1, e2). Therefore, the B2 and B23 were abnormal batches compared with other refined honey; the C23 was abnormal compared with other batches

of he-tuo honey. It ultimately meant that B2, B23 and C23 should be highlighted in real-world honey manufacturing to ensure the quality of honey intermediates and honeyed products. Therefore, the specific diagnosis was achieved by TAS1R2@AuNPs/SPCE biosensor combined with the MSPC algorithm in honey manufacturing.

3.5. End-to-end quality transfer principle in the real-world honey manufacturing

In traditional craftsmanship, the raw honey was processed by a low-temperature decompression process to remove impurities, reduce moisture and increase viscosity to obtain refined honey, and then obtained he-tuo honey by high-temperature sterilization. Therefore, the refining process was a critical segment in honey manufacturing, and understanding the principle of quality transfer in real-world manufacturing could be conducive to honey quality. The modalities of quality transfer from raw honey to refined honey and then to he-tuo honey were adopted to clarify the quality transfer principle. In the refining process, the critical material attributes (CMAs) of raw honey and critical process parameters (CPP) (such as temperature, pressure, etc.) had a significant influence on the CQAs of he-tuo honey. Finally, the principle of quality transfer was elucidated by KDE and box plot, and end-to-end quality transfer dataflow was established that contained physical, chemical and biological CQAs in honey manufacturing.

3.5.1. Quality transfer modality from raw honey to refined honey

The modality of quality transfer from raw honey to refined honey was uniquely characterized by KDE. Here, the independent variable (X) and the dependent variable (Y) represented the identical quality attributes of raw honey and refined honey, respectively (Fig. 5). From the perspective of physical quality attributes, the DV, CV and VM increased significantly, while the EM declined from raw honey to refined honey (Fig. 5a1-a4). Therefore, the above rheological properties played an indispensable role for inspectors in the front-end honey refining process, and experience individuals could determine whether the process was stable or the product was reliable through the rheological properties.

From a chemical perspective, the pH value increased gradually during the transition from raw honey to refined honey (Fig. 5b1). The pH value fluctuations of refined honey were formidable to observe, which indicated that the pH value of refined honey was more distinctly affected by raw honey; the higher the pH value of raw honey, the higher that of refined honey. Additionally, the undulation of moisture content was particularly pronounced from raw honey to refined honey, followed by other chemical quality attributes (Fig. 5b2-b6). It was worth noting that moisture content presented a downward tendency, while the pH value and contents of fructose, glucose, sucrose and maltose showed increasing trends. Consequently, we demonstrated that moisture content could directly affect pH value and sugar in the front-end honey refining process.

Furthermore, sugar-to-sugar ratios were investigated in-depth, which included the content ratio of fructose to glucose, sucrose to maltose, and monosaccharide to disaccharides (Fig. 5c1-c3). Interestingly, the fluctuation amplitude of disaccharides was much greater than that of monosaccharides from raw honey to refined honey; the ratio of monosaccharides to disaccharides in refined honey was negatively correlated with that of raw honey. Therefore, moisture content, pH value and four types of sugar were the primary factors affecting the quality transfer in honey manufacturing, and these factors were easily affected by the refining techniques.

3.5.2. Quality transfer regularity in the honey manufacturing

Based on the quality transfer in the front-end refining process, we continued to effectively explain the regularity of quality transfer from raw honey to refined honey to he-tuo honey through physical, chemical, and biological quality attributes (Fig. 5d1-e), the physical and chemical quality attributes were the same as Section 3.5.1 and the biological quality attributes were represented by relative variation values of current peak (Fig. 5e).

During the honey refining process, pH value, DV, CV, VM and sugar content continued to increase, while EM and moisture content decreased. Notably, the DV, CV and VM gradually improved in the front-end process, while the stability of EM became significantly worse. In the back-end refining process, although the moisture content progressively shrank, the sugar content and the relative variation value of the current peak remained essentially unchanged. The content of monosaccharides was 17 times higher than that of disaccharides, with the passage of refining time, the ratio of monosaccharides to disaccharides decreased gradually and finally remained constant. Furthermore, the regularity of quality transfer in honey manufacturing showed that the relative variation values of biosensing current peak were closely related to chemical quality attributes. The above results explained that the honey quality fluctuated greatly in the front-end refining process, while the effect of the back-end process was negligible.

3.5.3. End-to-end quality transfer dataflow in the honey manufacturing

The innovative end-to-end quality transfer dataflow map was presented in Fig. 6, which contained physical, chemical, and biological CQAs. it was a groundbreaking challenge for applying the dataflow to digitally characterize the principle of quality transfer in real-world honey manufacturing. The standardized data of physical, chemical and biological CQAs were extracted and the path coefficients were calculated by Eq. (S5).

In principle, the contribution rate of CQAs was too low when the path coefficient value was inferior to 0.20; due to the powerful collinearity of the datasets, the coefficient should be discarded and recalculated. In addition, the residual error was calculated to represent the interpretation rate of the principal component factors. The lower the residual error, the higher the interpretation rate; the number of factors ought to be re-selected when it was superior to 0.15. In the meantime, the correlation coefficients of the score matrix were further calculated to characterize the path coefficients between different refining processes; the refining process of honey was relatively stable when it was greater than 0.75.

Fortunately, the end-to-end quality transfer dataflow in real-world honey manufacturing was calculated and established through a large number of experimental data to further explain the principle of quality transfer from raw honey to refined honey to he-tuo honey. The number of principal component factors was 2, and their cumulative contribution rate was superior to 80%. This dataflow map showed that the path coefficients from CQAs to honey intermediates were all greater than 0.20, and the residual errors were all less than 0.15, which demonstrated the end-to-end quality transfer dataflow in honey manufacturing was effective and reliable. Specifically, the pH value of the refining process was mainly affected by the decline of moisture content, and the two CQAs were inversely proportional, so their path coefficients had the same varying tendency. Meanwhile, there was a negative correlation between moisture and sugar content, the variation of moisture path coefficient was opposite to that of monosaccharides and consistent with that of disaccharides. Besides, compared with other CQAs, the elastic modulus changed more dramatically. Remarkably, the information transmitted in the dataflow was consistent with the regularity of quality transfer in honey manufacturing, the path coefficient of raw honey to refined honey was minimal (0.6176), which confirmed that the front-end refining process of honey was relatively unstable.

Taken together, during the whole refining process, the moisture content was gradually evaporated by low-temperature decompression, high-temperature sterilization, and other processes, and the moisture content was reduced to a stable state, while the sugar content and pH value increased to a certain range. Meanwhile, the increase in sugar content directly affected the affinity relationship between honey and

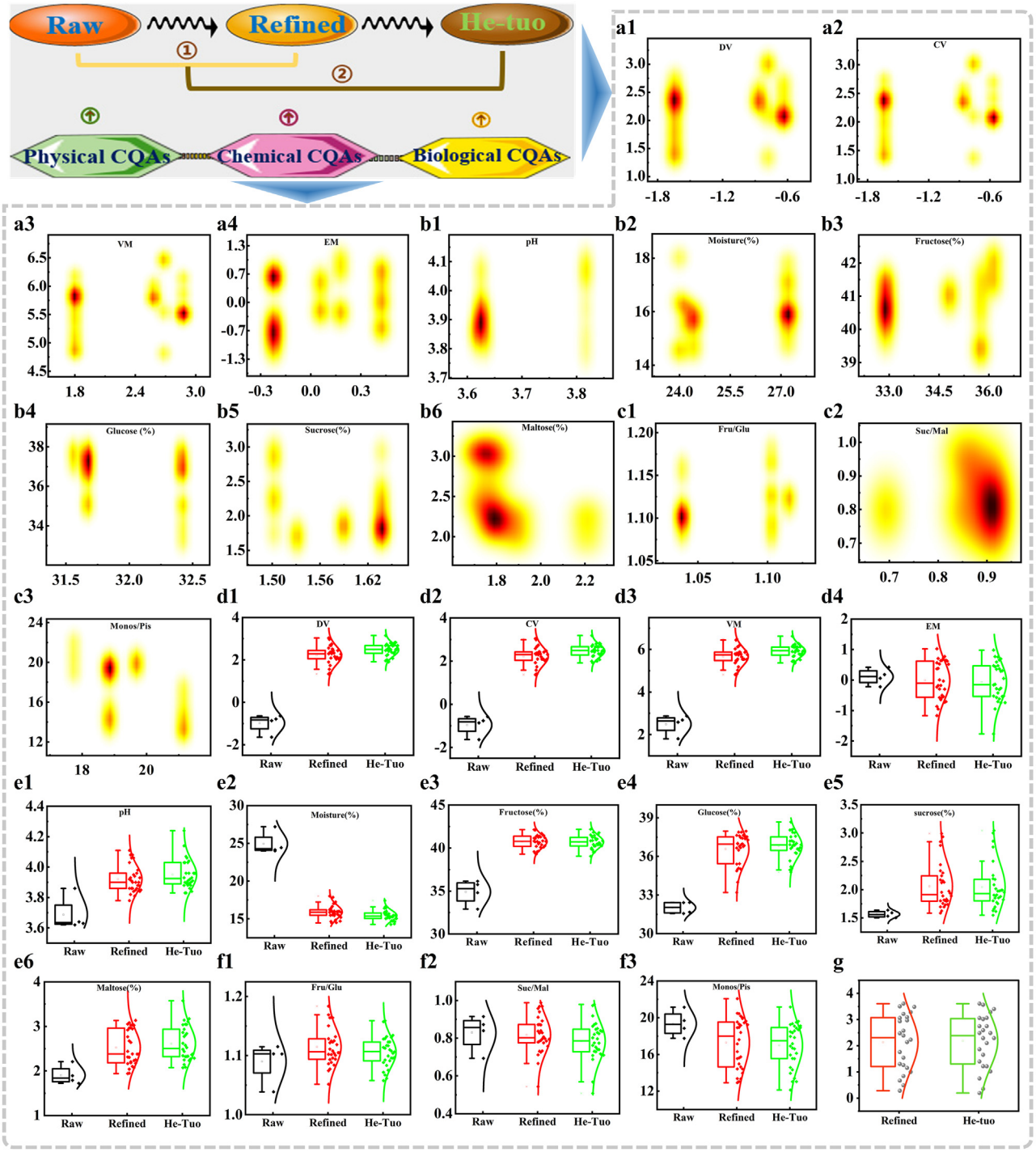

Fig. 5. Quality transfer diagram of honey manufacturing. (a1, a2, a3, a4) KDE diagram of DV, CV, VM and EM from raw honey (X-axis) to refined honey (Y-axis). (b1, b2, b3, b4, b5, b6) KDE diagram of pH value, moisture, fructose, glucose, sucrose and maltose from raw honey (X-axis) to refined honey (Y-axis). (c1, c2, c3) KDE diagram of the ratio of fructose to glucose, sucrose to maltose and monosaccharide to disaccharide from raw honey (X-axis) to refined honey (Y-axis). (d1, d2, d3, d4) Quality transfer diagram of DV, CV, VM and EM from raw honey to refined honey to he-tuo honey. (e1, e2, e3, e4, e5, e6) Quality transfer diagram of pH value, moisture, fructose, glucose, sucrose and maltose from raw honey to refined honey to he-tuo honey. (f1, f2, f3) Quality transfer diagram of the ratio of fructose to glucose, sucrose to maltose and monosaccharide to disaccharide from raw honey to refined honey to he-tuo honey. (g) Quality transfer diagram of the relative variation values of biosensing current peak from refined honey to he-tuo honey.

the TAS1R2 receptor. In addition, the honey gradually became sticky and thickened when the refining time increased, which ultimately affected its rheological characteristics. The end-to-end quality transfer dataflow was successfully applied to the manufacture of honey in the real world. The results indicated that the stability of the production process from raw honey to refined honey was the pivotal factor affecting product quality. Interestingly, the path coefficient determined which part of the refining process had a breakdown and then gave the warning signals in the honey manufacturing. More importantly, the end-to-end quality transfer dataflow embraced 9 CQAs of honey intermediate,

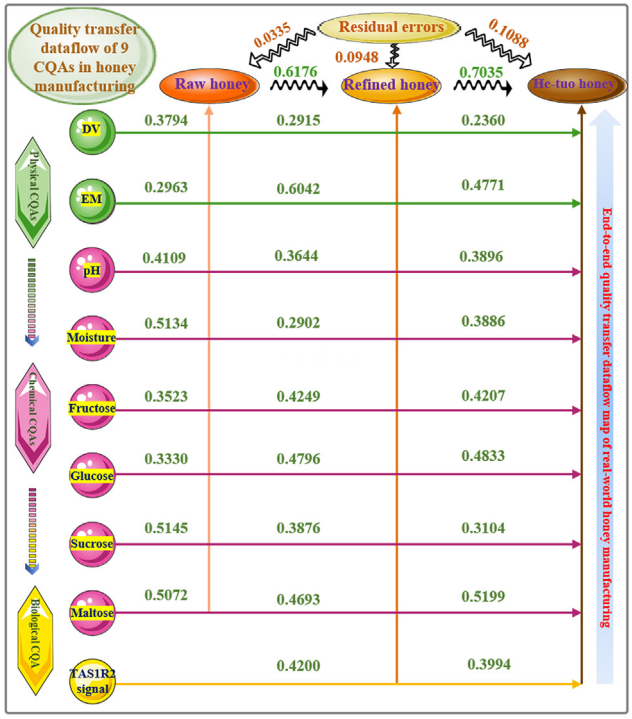

Fig. 6. An original end-to-end quality transfer dataflow map in honey manufacturing from the physical, chemical and biological CQAs.

which comprehensively dissected the quality transfer principle of honey manufacturing.

4. Conclusion

In this study, an original end-to-end dataflow engineering framework containing quality management and quality transfer for real-world honey manufacturing was developed to overcome the quality challenges. Firstly, 650 pivotal data points of physical and chemical quality attributes on 65 batches of honey intermediates were characterized by multiple sensors; eight physical and chemical critical quality attributes were discovered, which included DV, EM, pH, moisture, fructose, glucose, sucrose, and maltose. Furthermore, the TAS1R2@AuNPs/SPCE biosensor was innovatively assembled to identify biological critical quality attributes of honey intermediates, the powerful affinities between honey intermediates and TAS1R2 receptor were discovered and their K_D values were less than 10×10^{-8} M; Additionally, the abnormal batches of B2, B23 and C23 were demonstrated through TAS1R2@AuNPs/SPCE biosensor and MSPC algorithm. Finally, the quality transfer regularity of honey manufacturing was completely interpreted and the end-to-end dataflow containing physical, chemical and biological CQAs was successfully established to digitize the quality transfer principle in honey manufacturing. Gratifyingly, we discovered that the front-end refining process was relatively unstable and the back-end was a negligible influence on the quality of honey manufacturing. This framework in honey manufacturing will contribute to discovering the quality transfer principle in industrial innovation for intelligent manufacturing.

Author contribution

Xiaoyan Hu: Experiment, Data curation, Formal analysis, Investigation, Methodology, Software, Validation, Visualization, Writing - original draft, Writing - review &editing. Jingqi Zeng: Experiment, Data curation, Formal analysis, Investigation, Methodology, Software, Writing - original draft. Lijuan Ma: Writing - review &editing. Xiaomeng Wang: Writing - review &editing. Jing Du: Resources. Lu Yao: Resources. Zhisheng Wu: Conceptualization, Funding acquisition, Project administration, Supervision, Writing-review &editing.

Declaration of competing interest

The authors declare that they have no conflicts of interest in this work.

Acknowledgments

This work was co-supported by Excellent Young Scientists Fund of National Natural Science Foundation of China (82022073), Major scientific and technological R & D projects in Jiangxi Province (20203ABC28W018), National Natural Science Foundation of China (82274110), and the Fundamental Research Funds for the Central Universities (2022-JYB-JBZR-018, 2022-JYB-JBZR-019).

Supplementary materials

Supplementary material associated with this article can be found, in the online version, at doi:10.1016/j.fmre.2022.09.029.

References

[1] S. Ahmed, S.A. Sulaiman, A.A. Baig, et al., Honey as a potential natural antioxidant medicine: An insight into its molecular mechanisms of action, Oxid. Med. Cell Longev. 2018 (2018) 8367846.
[2] R.M. Swears, M. Manley-Harris, Composition and potential as a prebiotic functional food of a Giant Willow Aphid (Tuberolachnus salignus) honeydew honey produced in New Zealand, Food Chem. 345 (2021) 128662.
[3] S.K.T. Seraglio, M. Schulz, L.V. Gonzaga, et al., Current status of the gastrointestinal digestion effects on honey: A comprehensive review, Food Chem. 357 (2021) 129807.
[4] D. Wu, L. Chen, J. Teh, et al., Honeys with anti-inflammatory capacity can alter the elderly gut microbiota in an ex vivo gut model, Food Chem. 392 (2022) 133229.
[5] R.Y. Zhong, X. Xu, E. Klotz, et al., Intelligent manufacturing in the context of industry 4.0: A review, Engineering 3 (2017) 616–630.
[6] J. Zhou, P. Li, Y. Zhou, et al., Toward new-generation intelligent manufacturing, Engineering 4 (2018) 11–20.
[7] L. Gao, W. Shen, X. Li, New trends in intelligent manufacturing, Engineering 5 (2019) 619–620.
[8] Y. Zhou, J. Zang, Z. Miao, et al., Upgrading pathways of intelligent manufacturing in china: Transitioning across technological paradigms, Engineering 5 (2019) 691–701.
[9] T. Yang, X. Yi, S. Lu, et al., Intelligent manufacturing for the process industry driven by industrial artificial intelligence, Engineering 7 (2021) 1224–1230.
[10] L.J. Ma, J. Zhang, L. Lin, et al., Data-driven engineering framework with AI algorithm of Ginkgo Folium tablets manufacturing, Acta Pharm. Sin. B (2022), doi:10.1016/j.apsb.2022.08.011.
[11] H.X. Li, H. Si, Control for intelligent manufacturing: A multiscale challenge, Engineering 3 (2017) 608–615.
[12] M.C. Jaklevic, Quality issues prompt guidelines for compounded drug pharmacies, JAMA 324 (2020) 2357 -2357.
[13] L.J. Ma, Y.F. Zheng, J. Wang, et al., Development of MIF/IL-1β biosensors for discovery of critical quality attributes and potential allergic rhinitis targets from clinical real-world data by intelligent algorithm coupled with in vitro and vivo mechanism validation, Biosens. Bioelectron. 194 (2021) 113608.
[14] M.J. Aliaño-González, M. Ferreiro-González, E. Espada-Bellido, et al., A screening method based on Visible-NIR spectroscopy for the identification and quantification of different adulterants in high-quality honey, Talanta 203 (2019) 235–241.
[15] Q.Q. Li, J.Q. Zeng, L. Lin, et al., Low risk of category misdiagnosis of rice syrup adulteration in three botanical origin honey by ATR-FTIR and general model, Food Chem. 332 (2020) 127356.
[16] Q.Q. Li, J.Q. Zeng, L. Lin, et al., Mid-infrared spectra feature extraction and visualization by convolutional neural network for sugar adulteration identification of honey and real-world application, LWT 140 (2021) 110856.
[17] C.C. Li, Z.Y. Wang, L.J. Wang, et al., Biosensors for epigenetic biomarkers detection: A review, Biosens. Bioelectron. 144 (2019) 111695.
[18] R. Khaksarinejad, Z. Arabpour, L. RezaKhani, et al., Biomarker based biosensors: An opportunity for diagnosis of COVID-19, Rev. Med. Virol. 32 (2022) e2356.
[19] J. Vinoth Kumar, R. Karthik, S.M. Chen, et al., Design of novel 3D flower-like neodymium molybdate: An efficient and challenging catalyst for sensing and destroying pulmonary toxicity antibiotic drug nitrofurantoin, Chem. Eng. J. 346 (2018) 11–23.
[20] T.S.K. Sharma, K.Y. Hwa, Architecting hierarchal $Zn_3V_2O_8$/P-rGO nanostructure: Electrochemical determination of anti-viral drug azithromycin in biological samples using SPCE, Chem. Eng. J. 439 (2022) 135591.
[21] R. Balaji, S. Maheshwaran, S.M. Chen, et al., High-performance catalytic strips assembled with BiOBr Nano-rose architectures for electrochemical and SERS detection of theophylline, Chem. Eng. J 425 (2021) 130616.

[22] A. Abi, Z. Mohammadpour, X. Zuo, et al., Nucleic acid-based electrochemical nanobiosensors, Biosens. Bioelectron. 102 (2018) 479–489.
[23] B. Liu, J. Liu, Sensors and biosensors based on metal oxide nanomaterials, Trac-trend, Anal. Chem. 121 (2019) 115690.
[24] S.H. Oh, H. Altug, X. Jin, et al., Nanophotonic biosensors harnessing van der Waals materials, Nat. Commun. 12 (2021) 3824.
[25] A. Azzouz, L. Hejji, C. Sonne, et al., Nanomaterial-based aptasensors as an efficient substitute for cardiovascular disease diagnosis: Future of smart biosensors, Biosens. Bioelectron. 193 (2021) 113617.
[26] L. Chiang, B. Lu, I. Castillo, Big data analytics in chemical engineering, Annu. Rev. Chem. Biomol. 8 (2017) 63–85.
[27] A.V. Santos, A.R.A. Lin, M.C.S. Amaral, et al., Improving control of membrane fouling on membrane bioreactors: A data-driven approach, Chem. Eng. J. 426 (2021) 131291.
[28] Y.J. Liu, S. André, L. Saint Cristau, et al., Multivariate statistical process control (MSPC) using Raman spectroscopy for in-line culture cell monitoring considering time-varying batches synchronized with correlation optimized warping (COW), Anal. Chim. Acta 952 (2017) 9–17.
[29] H. Hadian, A. Rahimifard, Multivariate statistical control chart and process capability indices for simultaneous monitoring of project duration and cost, Comput. Ind. Eng. 130 (2019) 788–797.
[30] I.N. Pasias, K.G. Raptopoulou, G. Makrigennis, et al., Finding the optimum treatment procedure to delay honey crystallization without reducing its quality, Food Chem. 381 (2022) 132301.
[31] C.C. da Costa, R.G. Pereira, The influence of propolis on the rheological behaviour of pure honey, Food Chem. 76 (2002) 417–421.
[32] M.M. Cavia, M.A. Fernández-Muiño, S.R. Alonso-Torre, et al., Evolution of acidity of honeys from continental climates: Influence of induced granulation, Food Chem. 100 (2007) 1728–1733.
[33] A.C.D. Santos, F.C. Biluca, F. Braghini, et al., Phenolic composition and biological activities of stingless bee honey: An overview based on its aglycone and glycoside compounds, Food Res. Int. 147 (2021) 110553.
[34] J. Wu, Y. Duan, Z. Gao, et al., Quality comparison of multifloral honeys produced by Apis cerana cerana, Apis dorsata and Lepidotrigona flavibasis, LWT 134 (2020) 110225.
[35] K. Smith, E. Karimian Azari, T.E. LaMoia, et al., T1R2 receptor-mediated glucose sensing in the upper intestine potentiates glucose absorption through activation of local regulatory pathways, Mol. Metab. 17 (2018) 98–111.
[36] Y. Ben Shoshan-Galeczki, M.Y. Niv, Structure-based screening for discovery of sweet compounds, Food Chem. 315 (2020) 126286.
[37] J.Y. Jeong, Y.K. Cha, S.R. Ahn, et al., Ultrasensitive bioelectronic tongue based on the venus flytrap domain of a human sweet taste receptor, Acs Appl. Mater. Inter. 14 (2022) 2478–2487.
[38] I. Sarangadharan, A. Regmi, Y.W. Chen, et al., High sensitivity cardiac troponin I detection in physiological environment using AlGaN/GaN High Electron Mobility Transistor (HEMT) Biosensors, Biosens. Bioelectron. 100 (2018) 282–289.

Author profile

Xiaoyan Hu is a graduate student jointly trained by the Beijing University of Chinese Medicine and the Fujian University of Chinese Medicine. She mainly focuses on biosensor chips and quality control of intelligent manufacturing processes of Chinese Materia Medica.

Zhisheng Wu is a professor and Ph.D. supervisor at the Beijing University of Chinese Medicine (BUCM), and principal investigator and vice-dean of the Engineering Research Center for Pharmaceutics of Chinese Materia Medica and New Drug Development of the Ministry of Education in China. He received visiting chair professor of Minjiang scholars and the Excellent Young Scientists Fund of the National Natural Science Foundation of China. He has published more than 120 papers including *Bioresource Tech*, *J. Control Release*, and *Biosens. Bioelectron*, *Acta Pharmaceutica Sinica B*. He is awarded the Science and Technology Progress Award of Beijing, etc.